Attitude Observability of a Loosely-Coupled GPS/Visual Odometry Integrated Navigation Filter

Damien Dusha, Luis Mejias
Australian Research Centre for Aerospace Automation
Queensland University of Technology
Brisbane, Australia
{d.dusha,luis.mejias}@qut.edu.au

Abstract

We present a novel method for integrating GPS position estimates with position and attitude estimates derived from visual odometry using a scheme similar to a classic loosely-coupled GPS/INS integration. Under such an arrangement, we derive the error dynamics of the system and develop a Kalman Filter for estimating the errors in position and attitude. Using a control-based approach to observability, we show that the errors in both position and attitude (including yaw) are fully observable when there is a component of acceleration perpendicular to the velocity vector in the navigation frame. Numerical simulations are performed to confirm the observability analysis.

1 Introduction

In the last decade, considerable effort has been expended on vision-based navigation, the closely related Structure from Motion (SfM) and Simultaneous Localisation and Mapping (SLAM) problems. Schemes include the tracking and integration of feature points [Chiuso *et al.*, 2002] or local planar features [Calway, 2005], culminating in the stereo-vision systems demonstrated by Nister [Nister *et al.*, 2006] and on the Mars Exploration Rover [Maimone *et al.*, 2007]. For a Visual Odometry system without reference to external landmarks, the vehicle state estimates will drift with time. Methods to constrain the drift have been demonstrated using terrain maps [Lerner *et al.*, 2006] and visual landmark recognition [Kais *et al.*, 2004]. Using SLAM, one can build a local map of features and provide a bounded estimate of the vehicle's location within that map [Bryson and Sukkarieh, 2008]. Real-time SLAM implementations have been demonstrated using a hand-waved camera [Davison, 2003] and on an Unmanned Airborne Vehicle (UAV) [Bryson and Sukkarieh, 2007].

To prevent drift, SLAM requires re-observation of features to reduce the growth in localisation errors [Bryson and Sukkarieh, 2008]. In UAV missions where cross-country navigation is required, maintaining a flight path where past features can be observed may not be practical and therefore SLAM is of little utility. Whilst the problem of position for en-route navigation for airborne civilian applications can largely be solved with a low-cost GPS receiver, attitude (which is critical to the control of a UAV) is not yet so cost-effectively solved, with the cost of an Inertial Measurement Unit (IMU) still of same order of magnitude as the airframe itself. Since cameras are a common payload on a UAV, if vision-based attitude can provide reliable measurements, then there is the potential to remove the need for an IMU, or at least to be able to provide a backup measurement.

For a UAV operating at altitude, detecting the sky horizon has been demonstrated as a means to estimate the attitude of an aircraft. Todorovic [Todorovic *et al.*, 2003] demonstrated the use of the horizon as a control feedback signal for real-time pitch and roll stabilisation of a Micro Airborne System. Later, Gupta estimated yaw in addition to pitch and roll using the terrain profile at the horizon [Gupta and Brennan, 2008], though it has the limitation that a clear view of distinctive terrain is necessary.

Inertial sensors have a longstanding history for attitude determination. So-called Attitude and Heading Reference Systems (AHRS) typically consist of a complementary filter where the body angular rates measured using the gyros are analytically rotated to the navigation frame and integrated to calculate pitch, roll and yaw. Since the gyro measurements are integrated, any bias or noise on the sensors will cause the attitude solution to drift. The drift is constrained in the complementary filter by using the gravity vector measured with the accelerometers to obtain an independent measurement of pitch and roll [Farrell, 2008]. Hence, the ultimate accuracy of the pitch and roll estimates are constrained by quality of the accelerometers, commonly approximated as 1 milliradian per milli-g. Furthermore, drift in yaw is unconstrained without the aid of a magnetic compass or

other external measurement.

In an Inertial Navigation System (INS), measurements from the accelerometers may also be rotated from the body frame to a reference frame (using the integrated gyros as the attitude measurement) and integrated twice to estimate position. However, since position errors grow quadratically with time for accelerometer errors and cubically with time for gyro errors [Groves, 2007], unaided inertial navigation is impractical for more than a few seconds using low-cost sensors [Godha, 2006]. When integrated with GPS measurements, however, the position drift is constrained and under particular manoeuvres, the attitude of the vehicle (including yaw) may be recovered by virtue of the error dynamics of the integration scheme [Hong *et al.*, 2005; Rhee *et al.*, 2004].

As much of the emphasis in vision-based navigation research is on positioning where GNSS[1] is unavailable or denied, there is little research in combining GPS and vision-based measurements. Roberts [Roberts *et al.*, 2005] combines optical flow and focus of expansion measurements with GPS velocity and pseudo-attitude measurements to recover the attitude of a UAV. Ding [Ding *et al.*, 2009] fuses simplified optical flow measurements to assist estimation in a GPS/INS loop. Chatterji [Chatterji *et al.*, 1997] combines measurements of known visual runway markers (e.g. airport lights) with GPS to assist in the positioning of a aircraft relative to a runway for landing. The specific problem of determining camera rotations given known camera locations (i.e. GPS positions) was studied by Carceroni in terms of the number of correspondences necessary to determine a rotation solution [Carceroni *et al.*, 2006].

1.1 Contribution

In this paper, we propose a novel method for the integration of Visual Odometry with GPS in a manner similar to a loosely-coupled GPS/INS system. The error dynamics of the integration are derived and used as the process model for an error-state Kalman Filter. An observability analysis of the integration scheme is conducted, leading to the result that errors in position and attitude are fully observable when there is a component of acceleration perpendicular to the velocity vector. The observability is then demonstrated using a numerical analysis. Unlike other approaches to vision-based navigation, the integration scheme we propose does not require the use of an IMU, nor does it require the storage of image features or positions, making it a suitable for real-time implementation on modest computing hardware, subject to the requirements of the egomotion front-end.

[1]In this paper, GPS is synonymous with GNSS as virtually every commercially available GNSS receiver uses GPS and only a select few utilise GLONASS

1.2 Notation

The notation used in this paper is as follows:

An identity matrix of size k is denoted by $\mathbf{I}_k$.

The rotation matrix from the a-frame to the b-frame is denoted by $\mathbf{R}_a^b$.

γ_{ab}^c denotes a vector quantity γ of the b-frame with respect to the a-frame, expressed in terms of the c-frame.

$[\mathbf{A}]_\times$ is a skew-symmetric matrix constructed from vector $\mathbf{A}$ such that when multiplied by vector $\mathbf{B}$ the result is equivalent to the cross-product of $\mathbf{A}$ and $\mathbf{B}$, viz $[\mathbf{A}]_\times \mathbf{B} = \mathbf{A} \times \mathbf{B}$.

Time derivatives of a quantity are expressed using the dot notation (e.g. $\dot{\omega}_{ab}^c$).

Estimated or measured quantities are denoted with a tilde (e.g. $\tilde{\omega}_{ab}^c$).

In this paper, the b-frame is the body fixed frame, the n-frame is an earth-fixed local tangent frame (north, east, down) and the i-frame is the Earth-Centred Inertial (ECI) frame.

2 GPS/INS Attitude Observability

For several decades, it has been known that the errors from GPS and INS are complementary in nature [Groves, 2007]; GPS is a low-bandwidth but stable and bounded solution, whereas an INS provides a high-bandwidth solution but suffers from drift over time. In the simplest form of GPS/INS integration - so-called *uncoupled integration* - the INS solution is simply reset with the GPS solution on a periodic basis to prevent the accumulation of position and velocity errors. In this instance, the attitude solution is determined solely by the INS and therefore the yaw solution will forever drift with time.

A better solution to the GPS/INS integration problem can be found by examining how the errors of an INS propagate with time. It has been shown [Groves, 2007] that errors in the attitude solution of an INS propagate into errors in velocity. Therefore, errors in attitude can be observed through independent measurements of velocity (or position measurements over time), under particular motion conditions. Since GPS and INS user equipment were originally sold as separate systems without access to their internal sensors and algorithms, integration based on the error dynamics of the INS could only be done on the calculated GPS and INS solutions rather than the raw sensor measurements. Such an arrangement is known as *loosely-coupled integration* and is suboptimal compared with the direct use of GPS and IMU observables in a *tightly-coupled* integration. Furthermore, a tightly-coupled integration scheme has the advantage of using GPS measurements even when there are not enough satellites visible to calculate a standalone position solution.

Nevertheless, even loosely-coupled integration offers many benefits over a GPS or INS solution alone. Rhee

[Rhee *et al.*, 2004] conducted an observability analysis using a piecewise linear model and showed that non-constant acceleration allowed the observability of attitude angles other than angle about the jerk vector. Hong [Hong *et al.*, 2005] conducted a more extensive observability analysis of a loosely-coupled GPS/INS system using a linear time-varying observability approach similarly showed that all unobservable states in the constant acceleration case can be made observable through manoeuvring, including the lever arm between the GPS and the IMU.

In the following sections, we show the similarity between structure of the GPS/INS integration problem and the GPS/Visual Odometry (GPS/VO) integration problem and how a full attitude solution may be recovered.

3 GPS/Visual Odometry Integration

In a classic loosely-coupled GPS/INS integration (Figure 1), an Inertial Measurement Unit (IMU) provides specific force $\mathbf{f}_{ib}^b$ and angular rate ω_{ib}^b measurements to the Inertial Navigation System (INS). The INS calculates velocity $\mathbf{v}_{nb}^n$, position $\mathbf{r}_{nb}^n$ and attitude θ_{nb}^n in the navigation frame by integrating and rotating the IMU measurements. The Kalman Filter estimates the *error* of the INS solution, knowing the coupling of the errors between the states and using the error in position (i.e. the difference between the GPS and INS solutions) as the measurement to the KF. The errors estimated by the KF are used the correct the INS solution.

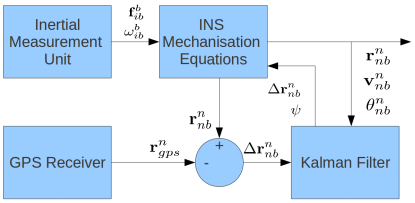

Figure 1: Classic Loosely-Coupled GPS/INS Error State Filter

The structure of the loosely-coupled GPS/Visual Odometry (GPS/VO) filter proposed in this paper (depicted in Figure 2) is substantially similar in structure to the GPS/INS in Figure 1. The IMU is replaced by a camera and egomotion calculation, which will yield velocity in the body frame $\mathbf{v}_{nb}^b$ and angular rate in the body frame ω_{nb}^b. The egomotion is then rotated integrated to obtain position and attitude in the navigation frame ("Visual Odometry"). The role of the Kalman Filter is exactly the same as the GPS/INS case, with the error dynamics adjusted for the Visual Odometry equations instead of the INS mechanisation equations.

For a single camera, egomotion is capable of recovering velocity and depth of a scene, though only up to a scale

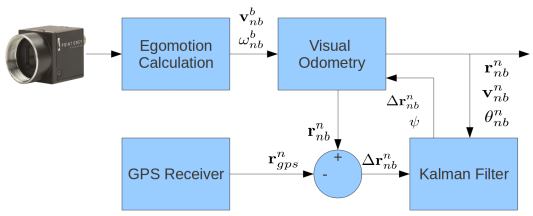

Figure 2: Proposed GPS/VO Error State Filter

factor [Chiuso *et al.*, 2002]. Where the visual odometry is calculated from stereo sequences, such as scheme implemented by Nister [Nister *et al.*, 2006], then the scale factor is estimated for the entire sequence. For the purposes of analysis presented in this paper, we assume that the scale factor is available (such as from stereo sequences) or is otherwise handled at the egomotion stage using (for example) GPS velocity measurements. Elegant handling of the scale factor in the filter framework is left for future research.

3.1 Visual Odometry

There are a number of methods that can be used for recovering the relative motion ("egomotion") between two scenes; see, for example, a recent survey on various methods by Bonin-Font and the references therein [Bonin-Font *et al.*, 2008]. From the velocity and rotation rate[2] provided by the egomotion, a position and attitude may be calculated using similar process to the INS mechanisation equations.

Assuming the angular rate is constant between updates, the attitude increment between frames may be calculated by [Groves, 2007; Ma *et al.*, 2004]

$$[\alpha]_\times = \int_t^{t+\tau} [\omega_{nb}^b]_\times dt \tag{1}$$

which is then used to calculate the relative rotation between frames:

$$\mathbf{A}_\tau = \exp([\alpha]_\times) \tag{2}$$

The attitude for time $t+\tau$ may then up calculated using

$$\mathbf{R}_b^n(t+\tau) = \mathbf{R}_b^n(t)\mathbf{A}_\tau \tag{3}$$

and the position may be updated by:

$$\mathbf{r}_{nb}^n(t+\tau) = \mathbf{r}_{nb}^n(t) + \int_t^{t+\tau} \mathbf{A}_\tau \mathbf{v}_{nb}^b dt \tag{4}$$

[2]Some algorithms provide a full relative rotation between frames rather than the angular rate. In this case, it may be directly substituted into Equation 3

3.2 Attitude Error Dynamics

We define the *misalignment* (or "attitude error") as the rotation error between the estimated attitude and the true attitude. That is:

$$\Delta\mathbf{R}_b^n \triangleq \tilde{\mathbf{R}}_b^n \mathbf{R}_n^b \tag{5}$$

If the misalignment angles are small, we may approximate the misalignment rotation matrix as:

$$\Delta\mathbf{R}_b^n \approx \mathbf{I}_3 - [\psi_{bn}^n]_\times \tag{6}$$

where ψ_{bn}^n is the small angle misalignment vector [Groves, 2007].

Defining $\mathbf{\Psi} = [\psi_{bn}^n]_\times$ and substituting Equation 6 into Equation 5 and rearranging:

$$\mathbf{\Psi} = \mathbf{I}_3 - \tilde{\mathbf{R}}_b^n (\mathbf{R}_b^n)^T \tag{7}$$

Differentiating Equation 7 with respect to time yields:

$$\dot{\mathbf{\Psi}} = -\dot{\tilde{\mathbf{R}}}_b^n (\mathbf{R}_b^n)^T - \tilde{\mathbf{R}}_b^n (\dot{\mathbf{R}}_b^n)^T \tag{8}$$

Defining $\mathbf{\Omega}_{nb}^b \triangleq [\omega_{nb}^b]_\times$ and noting that:

$$\dot{\mathbf{R}}_b^n = \mathbf{R}_b^n \mathbf{\Omega}_{nb}^b \tag{9}$$

$$\dot{\tilde{\mathbf{R}}}_b^n = \tilde{\mathbf{R}}_b^n \tilde{\mathbf{\Omega}}_{nb}^b \tag{10}$$

and substituting Equation 9 into 8 gives

$$\dot{\mathbf{\Psi}} = -\tilde{\mathbf{R}}_b^n [\tilde{\mathbf{\Omega}}_{nb}^b (\mathbf{R}_b^n)^T + (\mathbf{R}_b^n \mathbf{\Omega}_{nb}^b)^T] \tag{11}$$

Since $\mathbf{\Omega}_{nb}^b$ is a skew-symmetric matrix,

$$(\mathbf{\Omega}_{nb}^b)^T = -\mathbf{\Omega}_{nb}^b \tag{12}$$

Applying the matrix identity $\mathbf{B}^T\mathbf{A}^T = (\mathbf{AB})^T$ and rearranging yields

$$\dot{\mathbf{\Psi}} = -\tilde{\mathbf{R}}_b^n [\tilde{\mathbf{\Omega}}_{nb}^b (\mathbf{R}_b^n)^T - \mathbf{\Omega}_{nb}^b (\mathbf{R}_b^n)^T] \tag{13}$$

$$= -\tilde{\mathbf{R}}_b^n [\tilde{\mathbf{\Omega}}_{nb}^b - \mathbf{\Omega}_{nb}^b] (\mathbf{R}_b^n)^T \tag{14}$$

Defining:

$$\Delta\mathbf{\Omega}_{nb}^b \triangleq \tilde{\mathbf{\Omega}}_{nb}^b - \mathbf{\Omega}_{nb}^b \tag{15}$$

Substituting Equations 15 and 7 into 13:

$$\dot{\mathbf{\Psi}} = -\tilde{\mathbf{R}}_b^n \Delta\mathbf{\Omega}_{nb}^b (\mathbf{R}_b^n)^T \tag{16}$$

$$= [\mathbf{I}_3 - \mathbf{\Psi}] \mathbf{R}_b^n \Delta\mathbf{\Omega}_{nb}^b (\mathbf{R}_b^n)^T \tag{17}$$

Assuming that the product of two error terms are small:

$$\dot{\mathbf{\Psi}} = -\mathbf{R}_b^n \Delta\mathbf{\Omega}_{nb}^b (\mathbf{R}_b^n)^T \tag{18}$$

which, when expanding and matching coefficients yields the error state dynamics of the attitude:

$$\dot{\mathbf{\Psi}} = -\mathbf{R}_b^n \Delta\omega_{nb}^b \tag{19}$$

3.3 Position Error Dynamics

Define:

$$\dot{\mathbf{r}}_{nb}^n = \mathbf{v}_{nb}^n \tag{20}$$

and similarly for the estimated velocity:

$$\dot{\tilde{\mathbf{r}}}_{nb}^n = \tilde{\mathbf{v}}_{nb}^n \tag{21}$$

Defining the error in position as:

$$\Delta\mathbf{r}_{nb}^n \triangleq \tilde{\mathbf{r}}_{nb}^n - \mathbf{r}_{nb}^n \tag{22}$$

Differentiating Equation 22 yields:

$$\Delta\dot{\mathbf{r}}_{nb}^n = \dot{\tilde{\mathbf{r}}}_{nb}^n - \dot{\mathbf{r}}_{nb}^n \tag{23}$$

Substituting and expressing in the body frame:

$$\Delta\dot{\mathbf{r}}_{nb}^n = \tilde{\mathbf{R}}_b^n \dot{\tilde{\mathbf{r}}}_{nb}^b - \mathbf{R}_b^n \dot{\mathbf{r}}_{nb}^b \tag{24}$$

From Equation 7 and substituting into 24:

$$\Delta\dot{\mathbf{r}}_{nb}^n = [\mathbf{I}_3 - \mathbf{\Psi}] \mathbf{R}_b^n \dot{\tilde{\mathbf{r}}}_{nb}^b - \mathbf{R}_b^n \dot{\mathbf{r}}_{nb}^b \tag{25}$$

$$= \mathbf{R}_b^n (\tilde{\mathbf{v}}_{nb}^n - \mathbf{v}_{nb}^n) - \mathbf{\Psi}\mathbf{R}_b^n \tilde{\mathbf{v}}_{nb}^n \tag{26}$$

And defining:

$$\Delta\mathbf{v}_{nb}^n \triangleq \tilde{\mathbf{v}}_{nb}^n - \mathbf{v}_{nb}^n \tag{27}$$

After expanding and matching terms:

$$-\mathbf{\Psi}\mathbf{R}_n^b \tilde{\mathbf{v}}_{nb}^n = \mathbf{R}_b^n \left[\mathbf{v}_{nb}^b\right]_\times \psi \tag{28}$$

Therefore, the position error dynamics may be stated as:

$$\Delta\dot{\mathbf{r}}_{nb}^n = \mathbf{R}_b^n [\mathbf{v}_{nb}^b]_\times \psi + \mathbf{R}_b^n \Delta\mathbf{v}_{nb}^b \tag{29}$$

3.4 Navigation Error State Model

From Equations 29 and 19, the navigation error error model may be stated as:

$$\Delta\dot{\mathbf{r}}_{nb}^n = \mathbf{R}_b^n [\mathbf{v}_{nb}^b]_\times \psi + \mathbf{R}_b^n \Delta\mathbf{v}_{nb}^b \tag{30}$$

$$\dot{\mathbf{\Psi}} = -\mathbf{R}_b^n \Delta\omega_{nb}^b \tag{31}$$

Errors in position may be measured by the difference between the GPS and VO solutions:

$$\Delta\mathbf{r}_{nb}^n = \mathbf{r}_{gps}^n - \mathbf{r}_{vo}^n \tag{32}$$

Therefore, the error dynamics and the error measurements together form a Linear Time-Varying (LTV) system:

$$\begin{bmatrix} \Delta\dot{\mathbf{r}}^n_{nb} \\ \dot{\psi} \end{bmatrix} = \begin{bmatrix} \mathbf{0} & \mathbf{R}^n_b[\tilde{\mathbf{v}}^b_{nb}]_\times \\ \mathbf{0} & \mathbf{0} \end{bmatrix} \begin{bmatrix} \Delta\mathbf{r}^n_{nb} \\ \psi \end{bmatrix} + \begin{bmatrix} \mathbf{R}^n_b & \mathbf{0} \\ \mathbf{0} & -\mathbf{R}^n_b \end{bmatrix} \begin{bmatrix} \Delta\mathbf{v}^b_{nb} \\ \Delta\omega^b_{nb} \end{bmatrix} \quad (33)$$

$$[\Delta\mathbf{r}^n_{nb}] = \begin{bmatrix} \mathbf{I}_3 & \mathbf{0} \end{bmatrix} \begin{bmatrix} \Delta\mathbf{r}^n_{nb} \\ \psi \end{bmatrix} \quad (34)$$

The LTV system in Equation 33 is in the form required by the Kalman Filter, i.e.

$$\dot{\mathbf{x}}(t) = \mathbf{F}(t)\mathbf{x}(t) + \mathbf{G}(t)\mathbf{w}(t) \quad (35)$$

$$\mathbf{y}(t) = \mathbf{H}(t)\mathbf{x}(t) + \mathbf{v}(t) \quad (36)$$

One will note the similarity of the GPS/VO error state model in Equation 33 when compared to the classic loosely-coupled GPS/INS integration in the ECEF frame, neglecting lever arm and sensor bias terms, and assuming the contribution from error in gravity from position error is small [Groves, 2007]:

$$\dot{\mathbf{x}}_{INS}(t) = \begin{bmatrix} \mathbf{0} & \mathbf{I}_3 & \mathbf{0} \\ \mathbf{0} & -2\mathbf{\Omega}^e_{ie} & -\tilde{\mathbf{R}}^e_b[\tilde{\mathbf{f}}^b_{ib}]_\times \\ \mathbf{0} & \mathbf{0} & -\mathbf{\Omega}^e_{ie} \end{bmatrix} \begin{bmatrix} \Delta\mathbf{r}^e_{eb} \\ \Delta\mathbf{v}^e_{eb} \\ \psi^e_{eb} \end{bmatrix} \quad (37)$$

That is, the velocity error dynamics of the INS are very similar in structure to the position error dynamics of the visual odometry filter. The specific force term $\tilde{\mathbf{f}}^b_{ib}$ takes the place of the egomotion velocity term $\tilde{\mathbf{v}}^b_{nb}$ for the propagation in error due to misalignment. The exception is the addition of the Earth rate term $\mathbf{\Omega}^e_{ie}$ as the inertial sensors take measurements with respect to inertial frame, which is not measured using Visual Odometry.

3.5 Closed Loop Correction

The error dynamics for the Kalman Filter assume that the errors are small. In particular, the attitude error dynamics rely on the small angle assumption that may not be true if the VO solution is allowed to drift compared to the corrected solution. To prevent the growth in the errors in the VO solution, the error estimates from KF may be fed back into the VO solution. The disadvantage in performing loop closing is that there is no longer a vision-based solution that is independent of the GPS measurements.

Corrections to the VO solution are normally applied after a measurement update of the KF and follow the exact same form as the closed loop correction for a loosely-coupled GPS/INS solution [Groves, 2007], that is, the corrected navigation solution $\hat{\mathbf{R}}^n_b$ and $\hat{\mathbf{r}}^n_{nb}$ can be determined from the past Visual Odometry solution $\tilde{\mathbf{R}}^n_b$ and $\tilde{\mathbf{r}}^n_{nb}$ as follows:

$$\hat{\mathbf{R}}^n_b = (\Delta\hat{\mathbf{R}}^n_b)^T\tilde{\mathbf{R}}^n_b \quad (38)$$

$$\hat{\mathbf{r}}^n_{nb} = \tilde{\mathbf{r}}^n_{nb} - \Delta\mathbf{r}^n_{nb} \quad (39)$$

where $\Delta\mathbf{r}^n_{nb}$ is obtained directly from the Kalman Filter and $\Delta\hat{\mathbf{R}}^n_b$ is the direction cosine matrix formed from the attitude error ψ estimated by the Kalman Filter.

Once the corrections are applied, the error states in the Kalman Filter are set to zero but the covariance matrix remains unaltered as only the mean rather than the uncertainty is changed.

4 Observability of GPS/VO Integration

In the following section, we follow a similar methodology as Hong [Hong *et al.*, 2005] to analyse the observability of the GPS/VO integration. The analysis in this section assumes perfect (noise free) sensors, which is clearly the best possible theoretical case but is still of practical use – if states are not observable for the noise-free case, then they are not going to be made observable with the addition of noise.

4.1 Observability Definition

For this analysis, we adopt the definition of linear time-varying observability presented in [Chen, 1998]. Consider a linear time-varying system:

$$\dot{\mathbf{x}}(t) = \mathbf{F}(t)\mathbf{x}(t) \quad (40)$$

$$\mathbf{y}(t) = \mathbf{H}(t)\mathbf{x}(t) \quad (41)$$

where $\mathbf{F}(t)$ and $\mathbf{H}(t)$ are continuous functions of time defined over the domain $[-\infty, \infty]$ and are $n-1$ times continually differentiable, where n is the number of states in the state vector. Then the LTV system in Equation 40 is observable at t_0 if there exists a finite $t_1 > t_0$ such that

$$rank \begin{bmatrix} \mathbf{N}_0(t_1) \\ \mathbf{N}_1(t_1) \\ \vdots \\ \mathbf{N}_{n-1}(t_1) \end{bmatrix} = n \quad (42)$$

where

$$\mathbf{N}_0 = \mathbf{H}(t) \quad (43)$$

$$\mathbf{N}_{m+1}(t) = \mathbf{N}_m(t)\mathbf{F}(t) + \frac{d}{dt}\mathbf{N}_m(t) \quad (44)$$

$$m = 1, 2, \ldots, n-1 \quad (45)$$

Similarly, a linear time-invariant system is observable for every initial time if and only if the rank of the observability matrix

$$\mathbf{O} = \begin{bmatrix} \mathbf{H}^T & (\mathbf{HF})^T & (\mathbf{HF}^2)^T & \dots & (\mathbf{HF}^{n-1})^T \end{bmatrix}^T \tag{46}$$

is of rank n.

4.2 Observability Analysis

To simplify the observability analysis, we substitute $[\mathbf{R}_b^n \tilde{\mathbf{v}}_{nb}^b]_\times = [\tilde{\mathbf{v}}_{nb}^n]_\times$ into $\mathbf{F}(t)$. That is, we present the observability in terms of motion in the n-frame rather than the b-frame. Substituting the error dynamics system in Equation 33 into the LTV observability matrix in Equation 42 and simplifying yields

$$\mathbf{O} = \begin{bmatrix} \mathbf{I}_3 & \mathbf{0}_3 \\ \mathbf{0}_3 & [\tilde{\mathbf{v}}_{nb}^n]_\times \\ \mathbf{0}_3 & [\tilde{\mathbf{a}}_{nb}^n]_\times \\ \mathbf{0}_3 & \left[\ddot{\tilde{\mathbf{v}}}_{nb}^n\right]_\times \\ \mathbf{0}_3 & \left[\dddot{\tilde{\mathbf{v}}}_{nb}^n\right]_\times \\ \mathbf{0}_3 & \left[\ddddot{\tilde{\mathbf{v}}}_{nb}^n\right]_\times \end{bmatrix} \tag{47}$$

where $[\tilde{\mathbf{a}}_{nb}^n]_\times = \left[\dot{\tilde{\mathbf{v}}}_{nb}^n\right]_\times$.

In the following sections, we examine the observability of two special cases of the observability matrix in Equation 47 - constant velocity in the n-frame and constant acceleration in the n-frame.

Observability Under Constant Velocity

Under constant velocity, the LTV system in Equation 33 becomes an LTI system. Substituting Equation 33 into the LTI observability definition in Equation 46 and removing all zero rows yields

$$\mathbf{O} = \begin{bmatrix} 1 & 0 & 0 & 0 & 0 & 0 \\ 0 & 1 & 0 & 0 & 0 & 0 \\ 0 & 0 & 1 & 0 & 0 & 0 \\ 0 & 0 & 0 & 0 & -v_z & v_y \\ 0 & 0 & 0 & v_z & 0 & -v_x \\ 0 & 0 & 0 & -v_y & v_x & 0 \end{bmatrix} \tag{48}$$

which is of rank 3 for the zero-velocity case and is of rank 5 where the velocity is non-zero in one or more axes in the navigation frame.

Observability Under Constant Acceleration

Under constant acceleration, the LTV observability matrix is

$$\mathbf{O} = \begin{bmatrix} 1 & 0 & 0 & 0 & 0 & 0 \\ 0 & 1 & 0 & 0 & 0 & 0 \\ 0 & 0 & 1 & 0 & 0 & 0 \\ 0 & 0 & 0 & 0 & -v_z & v_y \\ 0 & 0 & 0 & v_z & 0 & -v_x \\ 0 & 0 & 0 & -v_y & v_x & 0 \\ 0 & 0 & 0 & 0 & -a_z & a_y \\ 0 & 0 & 0 & a_z & 0 & -a_x \\ 0 & 0 & 0 & -a_y & a_x & 0 \end{bmatrix} \tag{49}$$

which is of full rank, except where:

1. $\| \mathbf{v}_{nb}^n \| = 0$ (i.e. zero velocity case)
2. $\| \mathbf{a}_{nb}^n \| = 0$ (i.e. constant velocity case)
3. $\mathbf{v}_{nb}^n = k\mathbf{a}_{nb}^n$ (i.e. acceleration parallel to velocity vector)

For the case of a fixed-wing aircraft in flight, the attitude errors (and hence the attitude) are completely observable if there is a component of acceleration perpendicular to the velocity vector in the navigation frame. Hence, the manoeuvres required for observability of a GPS/VO integration are simpler compared to a GPS/INS as the latter requires jerk in order to make the attitude errors fully observable [Rhee *et al.*, 2004].

5 Implementation

To demonstrate the observability analysis, the proposed GPS/VO integration was implemented in MATLAB. In this section, we detail the approximations to the continuous-time system that were made in order to implement the system in discrete time.

For the Visual Odometry filter, the attitude increment α in Equation 1 is numerically integrated from the angular rate measurements ω_{nb}^b using the trapezoidal rule. Equation 2 is approximated with a fourth-order power series expansion [Groves, 2007]:

$$\mathbf{A}_\tau \approx \mathbf{I}_3 + (\mathbf{I}_3 - \frac{|[\alpha]_\times|^2}{6})[\alpha]_\times + (\mathbf{I}_3 - \frac{|[\alpha]_\times|^2}{24})([\alpha]_\times)^2 \tag{50}$$

with the attitude update calculated as

$$\mathbf{R}_b^n(+) = \mathbf{R}_b^n(-)\mathbf{A}_\tau \tag{51}$$

The position is updated using a rectangular integration of the velocity, transformed into the n-frame:

$$\mathbf{r}_{nb}^n(t+\tau) = \mathbf{r}_{nb}^n(t) + \frac{1}{2}\left(\mathbf{R}_b^n(-) + \mathbf{R}_b^n(+)\right)\mathbf{v}_{nb}^b(t)\tau \tag{52}$$

As the attitude update (and the applied corrections) are approximate, the attitude matrix requires periodic normalisation and orthogonalisation.

For the error state Kalman filter, the discrete-time state transition matrix $\mathbf{\Phi}_k$is calculated as [Farrell, 2008]

$$\mathbf{\Phi}_k = \exp\left(\mathbf{F}(t)\tau\right) \tag{53}$$

The errors estimated by the Kalman Filter are applied to the Visual Odometry solution after each measurement update in accordance with Equations 38.

5.1 Numerical Observability Analysis

To demonstrate some of the properties determined from the analytical observability analysis, we have performed a numerical analysis using the implementation presented in Section 5. In this analysis, we present the following scenarios, generated using the Aerospace Blockset in Simulink:

1. Constant velocity along the x-axis, including roll about the body frame
2. Constant velocity along the x-axis, including pitch about the body frame
3. Acceleration along the x-axis, with the initial velocity vector along the x-axis
4. Acceleration along the y-axis, with the initial velocity vector along the x-axis

In Scenarios 1-3, according to analytic observability analysis, at least one of the attitude parameters will not converge to the true value and will slowly diverge with time. In Scenario 4, all attitude components should be observable.

In all the scenarios presented, both the egomotion integration and the GPS measurements are performed at 20Hz[3]. White Gaussian noise is added to the body rates, velocity and GPS measurements with standard deviations of $5°/s$, $1m/s$ and $0.5m$ respectively. An initial random error is added to each of the states with a standard deviation of $30m$ in position and 15° in attitude.

Constant Velocity with Roll Manoeuvre

In this scenario, no accelerations are performed, but the vehicle performs a roll manoeuvre without altering the trajectory of the vehicle. Additionally, since the only change in attitude is roll and the body frame is aligned with the navigation frame, there is no change to the velocity in the b-frame. Figure 3 shows the angular rate of the platform and Figure 4 shows the attitude of the platform. From the attitude error in Figure 5, it can clearly be seen that the pitch and yaw angles quickly converge to their true values, but the roll (and the standard deviation of roll) diverges in a random walk-like pattern.

Figure 6 shows the yaw error for the first few seconds of the experiment. The rapid convergence to a steady-state figure from an initial error of more than 20° can be seen, along with a corresponding reduction in the standard deviation.

Constant Velocity with Pitch Manoeuvre

In Scenario 2, the trajectory of the vehicle remains at a constant velocity, but a pitching manoeuvre (Figure 7) causes both a change in attitude (Figure 9) and a change

[3]For example, the NovAtel OEMV-1 GPS receiver is capable of 20Hz

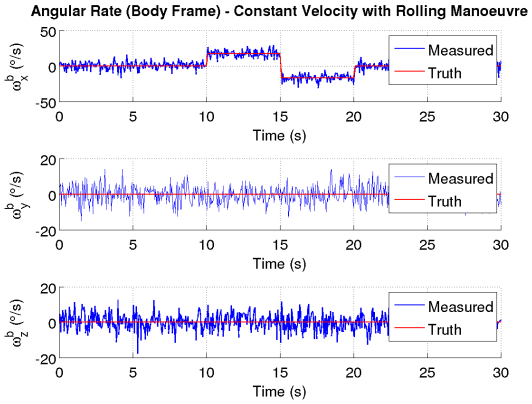

Figure 3: Scenario 1, Angular Rate Inputs with the platform performing a roll manoeuvre

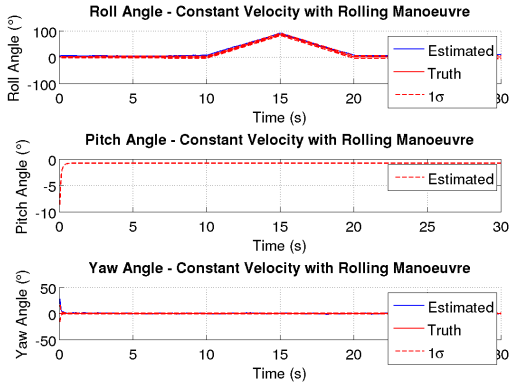

Figure 4: Scenario 1, Attitude Truth

to the velocity in the b-frame, as shown in Figure 8. However, as there is no acceleration in the n-frame, from the analytical observability analysis, we expect at least one of the attitude components to diverge. Figure 10 clearly shows the roll diverging whilst the roll and yaw remain observable throughout the manoeuvre.

Acceleration Parallel to Velocity

Scenario 3 has the platform accelerating in the same direction as the velocity vector (Figure 11) along the x-axis with the body frame aligned with the navigation frame. The resultant attitude plot in Figure 12 looks similar to the attitude error plots in the previous two scenarios, with the roll divergining with time. This outcome is consistent with the analytical observability analysis with the acceleration a scalar multiple of velocity.

Acceleration Non-Parallel to Velocity

In Scenario 4, a component of acceleration is added to the y-axis, perpendicular to the velocity vector along the x-axis, as shown in Figure 13. The alteration in trajec-

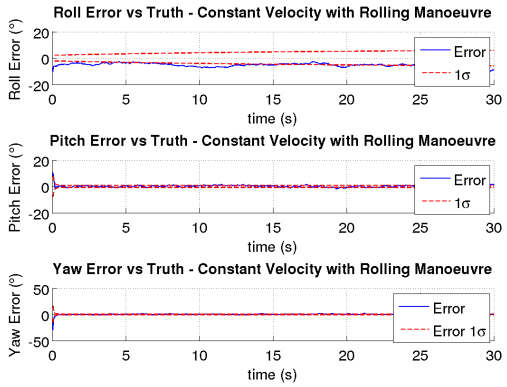

Figure 5: Scenario 1, Attitude Error

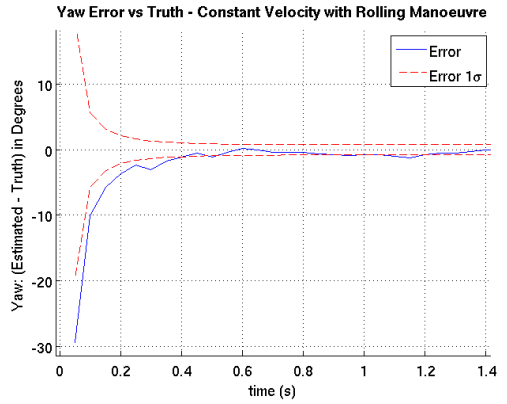

Figure 6: Scenario 1, Yaw Error - Initial converge

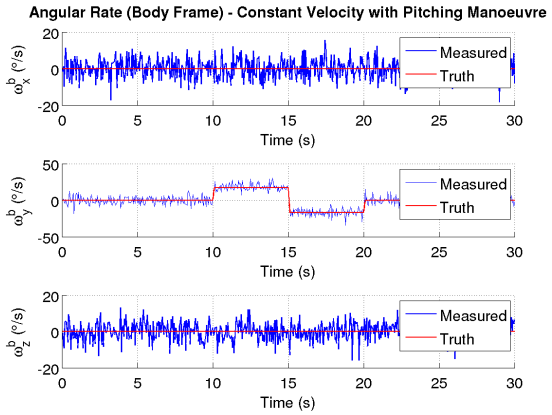

Figure 7: Scenario 2, Angular Rate Inputs

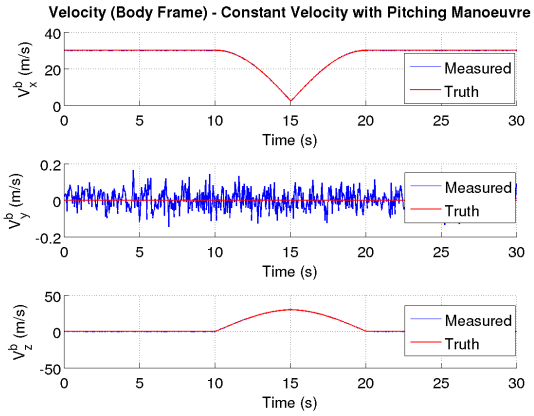

Figure 8: Scenario 2, Velocity in the b-frame. Note that although the velocity in the body frame is changing, the velocity in the navigation frame is not.

tory can be clearly be seen in the plan view in Figure 14. Throughout the manoeuvre, pitch and yaw remain observable, exhibiting results similar to the previous two scenarios. However, the roll error plot in Figure 15 deserves closer examination.

During the non-accelerating period between 0-5s, the roll error in Figure 15 shows no sign of converging. During the accelerating period from 5-10s, the roll error rapidly converges towards the truth value, consistent with roll being observable during this time. In the next period, from 10-15s, the platform is not accelerating and the roll does not coverage further. In the next period from 15-20s, the platform accelerates further and the roll converges back towards the truth again. This pattern is repeated, until the roll begins to diverge again during the period of no acceleration between 30-40s.

6 Conclusion and Future Work

In this paper, we proposed a novel integration of GPS and Visual Odometry, similar to a loosely-coupled GPS/INS integrated navigation solution. We derived the error dynamics of the visual odometry solution and designed a Kalman Filter for the estimation of the error states. Using a control-based approach to observability, we showed that the attitude is fully observable when there is a component of acceleration perpendicular to the velocity vector. The observability analysis was numerically demonstrated under various motion scenarios.

There are several avenues for future work. We are in the process of extending the filter to handle the scale of the scene and drift in scale factor, and to quantify the performance of the algorithm on real flight data. There is also scope for a direct-form implementation, using the visual odometry equations as the process model, and to implement the GPS/VO concept in a tightly-coupled configuration, directly using the pseudorange and carrier phase measurements from the GPS.

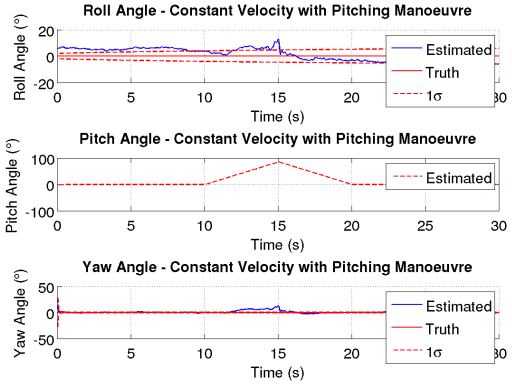

Figure 9: Scenario 2, Attitude Truth

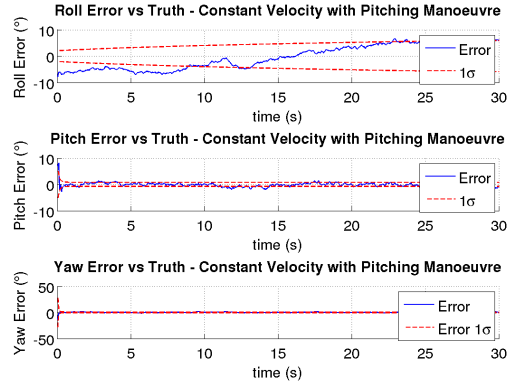

Figure 10: Scenario 2, Attitude Error. Note the continual growth in roll error.

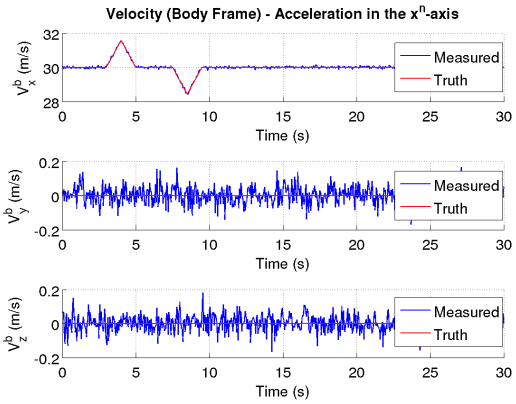

Figure 11: Scenario 3, Velocity in the b-frame

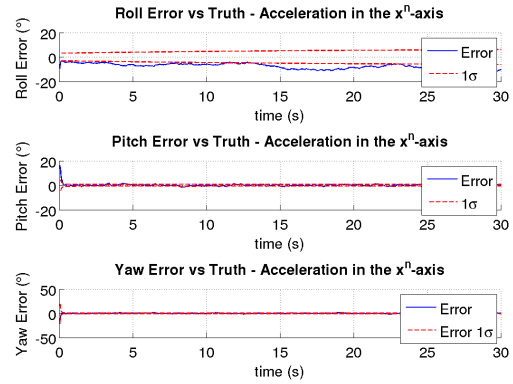

Figure 12: Scenario 3, Attitude Error

References

[Bonin-Font *et al.*, 2008] Francisco Bonin-Font, Alberto Ortiz, and Gabriel Oliver. Visual navigation for mobile robots: A survey. *Journal of Intelligent and Robotic Systems*, 53(3), November 2008.

[Bryson and Sukkarieh, 2007] Mitch Bryson and Salah Sukkarieh. Building a robust implementation of bearing-only inertial slam for a uav. *Journal of Field Robotics*, 24(1-2), 2007.

[Bryson and Sukkarieh, 2008] M. Bryson and S. Sukkarieh. Observability analysis and active control for airborne slam. *IEEE Transactions on Aerospace and Electronic Systems*, 44(1), 2008.

[Calway, 2005] A. Calway. Recursive estimation of 3d motion and surface structure from local affine flow parameters. *IEEE Transactions on Pattern Analysis and Machine Intelligence*, 27(4), 2005.

[Carceroni *et al.*, 2006] R. Carceroni, A. Kumar, and K. Daniilidis. Structure from motion with known camera positions. In *IEEE Conference on Computer Vision and Pattern Recognition*, 2006.

[Chatterji *et al.*, 1997] G.B. Chatterji, P.K. Menon, and B. Sridhar. GPS/machine vision navigation system for aircraft. *IEEE Transactions on Aerospace and Electronic Systems*, 33(3), 1997.

[Chen, 1998] Chi-Tsong Chen. *Linear System Theory and Design*. Oxford University Press, 3rd edition, 1998.

[Chiuso *et al.*, 2002] A. Chiuso, P. Favaro, Hailin Jin, and S. Soatto. Structure from motion causally integrated over time. *IEEE Transactions on Pattern Analysis and Machine Intelligence*, 24(4), 2002.

[Davison, 2003] A.J. Davison. Real-time simultaneous localisation and mapping with a single camera. In *IEEE International Conference on Computer Vision*, 2003.

[Ding *et al.*, 2009] W. Ding, J. Wang, S. Han, A. Almagbile, M. A. Garratt, A. Lambert, and J. J. Wang.

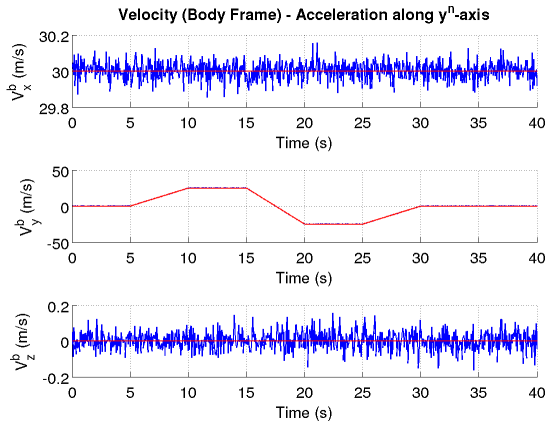

Figure 13: Scenario 4, Velocity in the b-frame

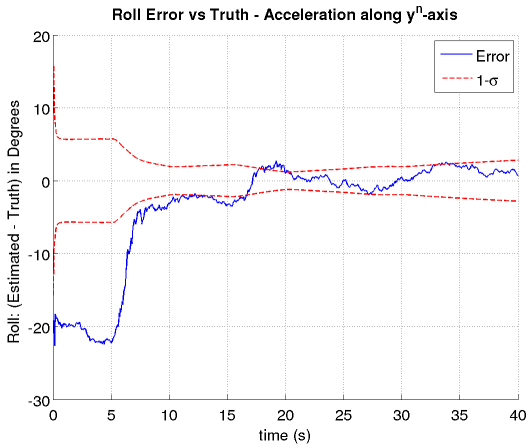

Figure 15: Scenario 4, Roll Error

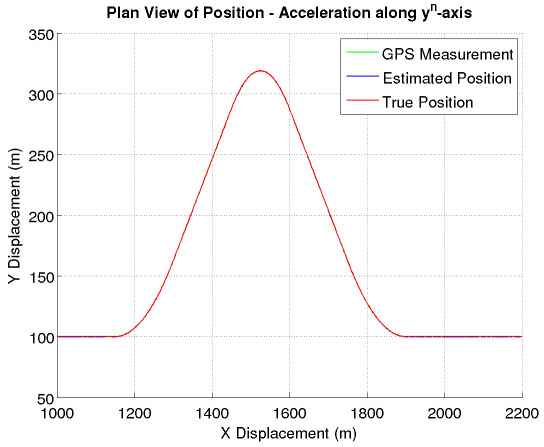

Figure 14: Scenario 4, Plan view of trajectory

Adding optical flow into the GPS/INS integration for UAV navigation. In *IGNSS Symposium*, 2009.

[Farrell, 2008] J.A. Farrell. *Aided Navigation: GPS with High Rate Sensors*. McGraw Hill, 2008.

[Godha, 2006] S. Godha. Performance evaluation of low cost mems-based imu integrated with gps for land vehicle navigation application. Master's thesis, University of Calgary, 2006.

[Groves, 2007] Paul D. Groves. *Principles of GNSS, Inertial, and Multi-Sensor Integrated Navigation Systems*. Artech House, 2007.

[Gupta and Brennan, 2008] V. Gupta and S. Brennan. Terrain-based vehicle orientation estimation combining vision and inertial measurements. *Journal of Field Robotics*, 25(3), 2008.

[Hong *et al.*, 2005] S. Hong, M. H. Lee, H. Chun, S. Kwon, and J.L. Speyer. Observability of error states in GPS/INS integration. *IEEE Transactions on Vehicular Technology*, 54(2), 2005.

[Kais *et al.*, 2004] M. Kais, S. Dauvillier, A. Fortellea, I. Masakid, and C. Laugier. Towards outdoor localization using GIS, vision system and stochastic error propagation. In *International Conference on Autonomous Robots and Agents*, 2004.

[Lerner *et al.*, 2006] R. Lerner, E. Rivlin, and H.P. Rotstein. Pose and motion recovery from feature correspondences and a digital terrain map. *IEEE Transactions on Pattern Analysis and Machine Intelligence*, 28(9), 2006.

[Ma *et al.*, 2004] Y. Ma, S. Soatto, J. Kosecka, and S. Sastry. *An Invitation to 3D Vision: From Images to Geometric Models*. Springer, 2004.

[Maimone *et al.*, 2007] M. Maimone, Y. Cheng, and L. Mattheis. Two years of visual odometry on the mars exploration rovers. *Journal of Field Robotics*, 43(3), 2007.

[Nister *et al.*, 2006] D. Nister, O. Naroditsky, and J. Bergen. Visual odometry for ground vehicle applications. *Journal of Field Robotics*, 23(1), 2006.

[Rhee *et al.*, 2004] I. Rhee, M.F. Abdel-Hafez, and J.L. Speyer. Observability of an integrated GPS/INS during maneuvers. *IEEE Transactions on Aerospace and Electronic Systems*, 40(2), 2004.

[Roberts *et al.*, 2005] P. Roberts, R. Walker, and P. O'Shea. Fixed wing uav navigation and control through integrated gnss and vision. In *AIAA Guidance Navigation and Control Conference*, 2005.

[Todorovic *et al.*, 2003] S. Todorovic, M.C. Nechyba, and P.G. Ifju. Sky/ground modeling for autonomous MAV flight. In *IEEE International Conference on Robotics and Automation*, 2003.